J. Am. Soc. Mass Spectrom. (2019) 30:1867–1880
DOI: 10.1007/s13361-019-02231-5

FOCUS: HONORING HELMUT SCHWARZ´S ELECTION TO THE NATIONAL ACADEMY OF SCIENCES: RESEARCH ARTICLE

Gas-Phase Synthesis and Reactivity of Ligated Group 10 Ions in the Formal +1 Oxidation State

Kim Greis,[1,2,3] Yang Yang,[1] Allan J. Canty,[4] Richard A. J. O'Hair[1]

[1]School of Chemistry and Bio21 Molecular Science and Biotechnology Institute, The University of Melbourne, Parkville, Victoria 3010, Australia
[2]Institut für Chemie, Humboldt-Universität zu Berlin, Brook-Taylor Straße 2, 12489, Berlin, Germany
[3]Fritz-Haber-Institut der Max-Planck-Gesellschaft, Faradayweg 4-6, 14195, Berlin, Germany
[4]School of Natural Sciences – Chemistry, University of Tasmania, Private Bag 75, Hobart, Tasmania 7001, Australia

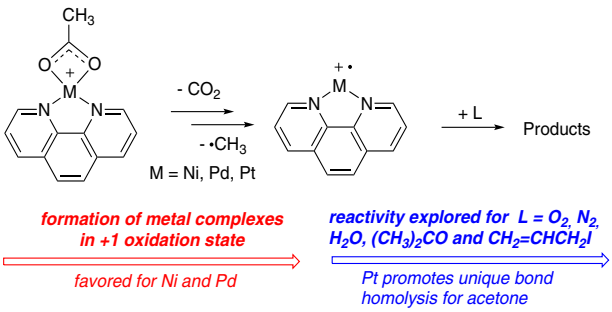

Abstract. Electrospray ionization of the group 10 complexes $[(phen)M(O_2CCH_3)_2]$ (phen=1,10-phenanthroline, M = Ni, Pd, Pt) generates the cations $[(phen)M(O_2CCH_3)]^+$, whose gas-phase chemistry was studied using multistage mass spectrometry experiments in an ion trap mass spectrometer with the combination of collision-induced dissociation (CID) and ion-molecule reactions (IMR). Decarboxylation of $[(phen)M(O_2CCH_3)]^+$ under CID conditions generates the organometallic cations $[(phen)M(CH_3)]^+$, which undergo bond homolysis upon a further stage of CID to generate the cations $[(phen)M]^{+\bullet}$ in which the metal center is formally in the +1 oxidation state. In the case of $[(phen)Pt(CH_3)]^+$, the major product ion $[(phen)H]^+$ was formed via loss of the metal carbene $Pt{=}CH_2$. DFT calculated energetics for the competition between bond homolysis and $M{=}CH_2$ loss are consistent with their experimentally observed branching ratios of 2% and 98% respectively. The IMR of $[(phen)M]^{+\bullet}$ with O_2, N_2, H_2O, acetone, and allyl iodide were examined. Adduct formation occurs for O_2, N_2, H_2O, and acetone. Upon CID, all adducts fragment to regenerate $[(phen)M]^{+\bullet}$, except for $[(phen)Pt(OC(CH_3)_2)]^{+\bullet}$, which loses a methyl radical to form $[(phen)Pt(OCCH_3)]^+$ which upon a further stage of CID regenerates $[(phen)Pt(CH_3)]^+$ via CO loss. This closes a formal catalytic cycle for the decomposition of acetone into CO and two methyl radicals with $[(phen)Pt]^{+\bullet}$ as catalyst. In the IMR of $[(phen)M]^{+\bullet}$ with allyl iodide, formation of $[(phen)M(CH_2CHCH_2)]^+$ was observed for all three metals, whereas for M = Pt also $[(phen)Pt(I)]^+$ and $[(phen)Pt(I)_2(CH_2CHCH_2)]^+$ were observed. Finally, DFT calculated reaction energetics for all IMR reaction channels are consistent with the experimental observations.

Keywords: Decarboxylation, Organoplatinum, Collision-induced dissociation, Ion-molecule reaction, Electrospray ionization, Mechanism, DFT calculation

Received: 19 February 2019/Revised: 14 April 2019/Accepted: 16 April 2019/Published Online: 10 June 2019

Introduction

Complexes of the group 10 metals are widely used as catalysts to facilitate transformations of organic substrates. For example, palladium-catalyzed cross-coupling reactions, which form C–X bonds (X = C, N, O, S, etc.), have revolutionized synthetic chemistry [1]. While oxidation states of 0 and +2 are commonly invoked in the catalytic reactions of these metals, there is a growing interest in the chemistry of other oxidation states [2]. The +1 oxidation state of nickel is

Dedicated to Professor Helmut Schwarz on the occasion of his election to the National Academy of Sciences and in recognition of his many important contributions to research in gas-phase ion chemistry and mass spectrometry and to promoting the internationalization of science via his Presidency of the Humboldt Foundation.

Kim Greis is on leave from Humboldt-Universität zu Berlin.

Electronic supplementary material The online version of this article (https://doi.org/10.1007/s13361-019-02231-5) contains supplementary material, which is available to authorized users.

Correspondence to: Richard O'Hair; *e-mail:* rohair@unimelb.edu.au

well established as playing a key role in catalysis [3], the structural aspects of Ni(I) complexes have been recently reviewed [4], and activation of small molecules by Ni(I) has been highlighted [5]. While Pd(I) and Pt(I) binuclear complexes are known [2, 6], only recently has the monomeric Pd(I) complex $[Pd(PtBu_3)_2][PF_6]$ been isolated and shown to catalyze the oxidative cross-coupling of arylantimony and arylboron nucleophiles [7]. With the resurgence of photoredox chemistry in organic synthesis, Ni(I) complexes are often invoked as key intermediates in catalytic cycles [8–10] and the gas-phase IR spectroscopy [11, 12] and chemistry [13, 14] of several ligated Ni(I) complexes have been reported.

Mass spectrometry-based techniques have been developed over the past 50 years to provide fundamental structural, mechanistic, and energetic information about intermediates and reactions associated with metal-mediated processes [15–18]. Professor Schwarz has been one of the key pioneers in this area, where he has shed light on mechanistic aspects of C–H bond activation in methane [19, 20] and developed a number of important concepts including "remote functionalization" [21] and "two-state reactivity" [22]. Gas-phase studies can provide powerful insights into catalytic cycles since they reveal details on elementary steps that can be difficult to study under typical conditions used for catalysis [23, 24]. While the gas-phase chemistry of bare monoatomic group 10 cations has been extensively studied by Schwarz [25, 26], Armentrout [27–29], and others [30], previous work on the reactions of $[((C_6H_5)_3P)_nAu]^+$ with iodobenzene has shown that ligation can have a profound effect on reactivity, with the bare cation ($n = 0$) undergoing a range of reactions, the monoligated ($n = 1$) complex selectively undergoing C–I bond activation and the bisligated complex ($n = 2$) being unreactive [31]. Thus, we were interested in developing a gas-phase synthesis of ligated group 10 cations in the formal oxidation state of +1. We chose the $[(phen)M(O_2CCH_3)]^+$ complexes as suitable precursors since the 1,10-phenanthroline (phen) ligand has been widely used in condensed phase synthetic and catalytic studies [32]; our previous work has shown that these complexes are readily generated via ESI-MS and decarboxylate upon CID [33] to generate organometallic cations, $[(phen)M(CH_3)]^+$, which undergo a number of interesting reactions of relevance to catalysis [34–39]; CID of related cations suggest that bond homolysis should occur [40]. Here, we examine the use of bond homolysis reactions of $[(phen)M(CH_3)]^+$ to generate the cations $[(phen)M]^{+\bullet}$ for subsequent ion-molecule reaction (IMR) studies. This approach is complementary to that of Parker and Gronert, who generated the ligated nickel radical cations $[(phen)_nNi]^{+\bullet}$ ($n = 1$ and 2) via electron transfer dissociation (ETD) to the dication $[(phen)_2Ni]^{2+}$ [41]. Our aim is to compare the bimolecular reactivity of ligated M(I) cations for Ni, Pd, and Pt, which has not yet been achieved due to the challenges of generating these reactive intermediates in the condensed phase where they can be depleted via disproportionation or other reactions. The IMR we have examined include those with background water, O_2 and N_2 and the reagents acetone and allyl iodide. Acetone was chosen for the following reasons: (i) previous studies on its reaction with the bare atomic cations Ni^+ and Pd^+ have revealed that C–C bond activation occurs [42–46]; (ii) our previous study on the reactions of $[(phen)M(CH_3)]^+$ with acetone uncovered a catalytic cycle [47]; (iii) metal complexes in low oxidation states react with acetone to form a coordinated ketyl radical that undergoes subsequent radical-driven fragmentation [48]. Allyl iodide was chosen since its C–C bond coupling reactions often proceed via metal-mediated C–I bond activation [49, 50].

Experimental

Chemicals from the following suppliers were used without further purification: (i) Merck, methanol (HPLC grade for ESI/MS^n experiments); (ii) Chem-Supply, acetone (AR grade); (iii) Cambridge Isotope Laboratories, acetone-d_6; (iv) Sigma-Aldrich, allyl iodide.

While the precursors $[(phen)Ni(O_2CCH_3)_2]$ and $[(phen)Pd(O_2CCH_3)_2]$ were available from a previous study [35], $[(phen)Pt(O_2CCH_3)_2]$ was synthesized via a literature procedure [51–53].

Mass Spectrometry Experiments

Mass spectrometric experiments were conducted on a Thermo Scientific linear ion trap (LTQ) spectrometer modified to allow IMR studies to be undertaken [54, 55]. It has been demonstrated that collisions with the helium bath gas quasi-thermalize ions to room temperature under IMR conditions [56]. Since the product complexes of interest are reactive towards background gases, precursor ions were mass selected with a 1-Da isolation window. Thus, the distinction between complexes with similar mass-to-charge ratios such as $[(phen)^{60}Ni(CH_3)]^+$ and $[(phen)^{58}Ni(OH)]^+$ was achieved by monoisotopic mass selection (^{58}Ni, ^{106}Pd, and ^{195}Pt). While isolation of a single isotope from the isotope manifold does lead to an overall decrease in the signal, the dynamic range of the ion trap is sufficient to carry out the desired MS^n experiments ($n = 2$–5).

The organometallic acetate cations, $[(phen)M(O_2CCH_3)]^+$, were generated via direct electrospray ionization (ESI) of the acetate complexes $[(phen)M(O_2CCH_3)_2]$ dissolved in methanol (~ 0.1 mM). The analyte solution was injected into the ESI source at a flow rate of 10 μL/min. ESI conditions used were the following: spray voltage 4.0 kV, capillary temperature 300 °C, nitrogen sheath gas flow rate ca. 10 arbitrary units. The three-coordinate organometallic cations, $[(phen)M(CH_3)]^+$, were generated by low-energy CID of the mass-selected complexes, $[(phen)M(O_2CCH_3)]^+$, in the linear ion trap. Low-energy CID on the mass-selected $[(phen)M(CH_3)]^+$ can be used to generate the two-coordinate organometallic cations, $[(phen)M]^{+\bullet}$. The helium bath gas was used as the collision gas and the CID conditions used included a Q value of 0.25 and an excitation time of 30 ms, with the normalized collisional energy varied from 13 to 20 (arbitrary units). The implementation of IMR in the

modified LTQ has been previously described in detail (see references [54, 55]). In brief, IMR of the mass-selected organometallic cations, $[(phen)M]^{+\cdot}$ with the neutral reagents, were carried out in a series of MS^4 experiments. The liquid neutral reagent (acetone or allyl iodide) is injected at flow rates of 10–100 μL/h directly into a stainless steel line that supplies helium to the linear ion trap. The line is heated to the boiling point of the liquid to promote vaporization. The flow of helium is controlled to 230 cm^3/min, and thus the composition of the liquid reagent/helium mixture can be calculated using the known molar flow rates of helium and the neutral reagent. Since the helium pressure regulator to control the flow of gas into the ion trap is bypassed, the helium pressure is instead manually controlled by matching the pressure in the vacuum chamber surrounding the ion trap, measured using the ion gauge, to that under normal operating conditions ($\approx 7–8 \times 10^{-6}$ Torr). This corresponds to a pressure of $\approx 2 \times 10^{-3}$ Torr inside the linear ion trap. During the IMR, no CID voltage was applied (i.e., NCE = 0) and appropriate reaction time was chosen to observe the formation of product ions. Acetone was introduced in the ion trap via the helium inlet line at a flow rate of 10 μL/h for the reactions with the Ni and Pd cations and 100 μL/h for the Pt cations. IMR between $[(phen)M]^{+\cdot}$ and allyl iodide were carried out with a reaction time of 30 ms. Allyl iodide was introduced via the helium inlet line at a flow rate of 50 μL/h.

Computational Methods

Structures of all reactants, transition states, and intermediates were fully optimized using the software Gaussian 09 [57]. If not stated otherwise, the M06 DFT functional [58] employing the SDD effective core potentials (ECPs) for Pt, Pd, and Ni [59, 60] and the 6-31G(d) basis set for all other atoms were used [61]. Some structures were re-optimized using Gaussian16 [62] and the B3LYP DFT functional [63] with Grimme's D3 correction [64, 65] with the basis set SDD for Pt, Pd, and Ni and the 6-311G(d) basis set for all other atoms [66]. Vibrational frequency calculations were performed to confirm stationary points as minimal (no imaginary frequency) or transition states (one imaginary frequency) and to obtain the zero-point energy (ZPE) corrections. Each transition state was connected to two minima by intrinsic reaction coordinate (IRC) calculations. A series of single-point energy calculations were carried out using the ORCA suite of programs [67] using the semi-empirical hybrid functional ωB97X-D3 [68] and double-hybrid functionals PWPB95-D3 [69] and DSDPBEP86-D3 [70], with the RI approximation [71] on the MP2 part of the calculation, with the basis set def2-TZVPP and ECPs on Pd and Pt [72]. Semi-empirical double-hybrid functionals have been chosen over non-empirical ones because the former has been shown to be more robust [73]. The optimized structures with the B3LYP-D3/6-311G(d) level of theory were used for the single-point energy calculations.

The thermodynamic parameter used to determine the likelihood of low-pressure unimolecular and bimolecular reactions to proceed was the reaction energy, *Δ(E+ZPE)*. The precursor ions undergo multiple collisions with the helium bath gas resulting in slow "heating" until fragmentation occurs, in the case of low energy CID [74]. Thus, the effective temperature is not known and will be different for each system. For the IMR, Dau et al. have highlighted that the relevant thermodynamic parameter to use for low-pressure bimolecular reactions is the reaction energy rather than the Gibbs free energy since the computed entropy of the reactants is not a good measure of the entropy at the entrance channel [75].

With regard to the multiplicities of the organometallic cations, $[(phen)M(CH_3)]^+$, we found that the ground states are singlets in the case of Pd and Pt, but that the ground state of $[(phen)Ni(CH_3)]^+$ is a triplet. This is consistent with the related $[(bipy)M(CH_3)]^+$ cations, where the ground state is a singlet for Pd and Pt and a triplet for Ni [76].

Results and Discussion

Bond Homolysis vs. Carbene Formation

Electrospray ionization of $[(phen)M(O_2CCH_3)_2]$ (M=Ni, Pd, Pt) complexes dissolved in methanol in the positive ion mode results in the formation of the mononuclear cationic complexes $[(phen)M(O_2CCH_3)]^+$. CID of these mass-selected complexes results in the formation of the methyl complexes $[(phen)M(CH_3)]^+$ as previously described (Fig. S1, Eq. (1)) [34, 35]. Besides decarboxylation, acetoxyl loss is another channel for M = Ni, Pd, resulting in the formation of the cationic complexes, $[(phen)M]^{+\cdot}$, where the metal is formally in the oxidation state +1 (Eq. (2)). As noted previously [34], the remaining ions observed in the mass spectra arise from IMR between the fragment ions and the background gases H_2O, N_2, and O_2. Thus, the complexes $[(phen)M(CH_3)]^+$ form adducts with dinitrogen for M = Pt (Eq. (3)) and with water for M = Pd and Pt (Eq. (4)). $[(phen)M(CH_3)]^+$ undergoes hydrolysis resulting in the formation of $[(phen)M(OH)]^+$ for M = Ni and Pt (Eq. (5)). For the short reaction time associated with these CID reactions, $[(phen)M]^{+\cdot}$ forms adducts with water and dioxygen only for M = Ni (Eq. (6)).

$$[(phen)M(O_2CCH_3)]^+ \rightarrow [(phen)M(CH_3)]^+ + CO_2 \quad (M = Ni, Pd, Pt) \tag{1}$$

$$[(phen)M(O_2CCH_3)]^+ \rightarrow [(phen)M]^{+\bullet} + CH_3CO_2\bullet \quad (M = Ni, Pd) \tag{2}$$

$$[(phen)Pt(CH_3)]^+ + N_2 \rightarrow [(phen)Pt(CH_3)(N_2)]^+ \tag{3}$$

$$[(phen)M(CH_3)]^+ + H_2O \rightarrow [(phen)M(CH_3)(OH_2)]^+ \quad (M = Pd, Pt) \tag{4}$$

$$[(phen)M(CH_3)]^+ + H_2O \rightarrow [(phen)M(OH)]^+ + CH_4 \quad (M = Ni, Pt) \tag{5}$$

$$[(phen)M]^{+\bullet} + L \rightarrow [(phen)M(L)]^{+\bullet} \tag{6}$$

Upon CID, the mass-selected complexes $[(phen)M(CH_3)]^+$ lose a methyl radical to form $[(phen)M]^{+\cdot}$ (Figure 1, Eq. (7)). However, for M = Pt, the loss of a methyl radical is only a minor pathway. The major pathway is the loss of $Pt{=}CH_2$ to generate the protonated ligand phenanthroline $[(phen)H]^+$ (*m/z* 181, Eq. (8)), which is detected in the mass spectrum (Figure 1c). Butschke and Schwarz reported a related reaction in the CID of $[(bipy)Pt(CH_3)]^+$ [76]. The organometallic cation $[(phen)Pt]^{+\cdot}$ (Eq. (7)) and the carbene $Pt{=}CH_2$ (Eq. (8)) are formed with branching ratios of 2% and 98% respectively. Although the thermochemistry of the neutral metal carbenes is not known for all group 10 metals, the $Pt{=}CH_2$ bond dissociation energy has been determined to be 446 kJ mol^{-1} [77], which highlights that it is a particularly stable species.

$$[(phen)M(CH_3)]^+ \rightarrow [(phen)M]^{+\bullet} + {\bullet}CH_3 \tag{7}$$

$$[(phen)M(CH_3)]^+ \rightarrow [(phen)H]^+ + M{=}CH_2 \quad (M = Pt) \tag{8}$$

To better understand the competing fragmentation pathways for $[(phen)M(CH_3)]^+$, DFT calculations have been performed to compare the energetics for bond homolysis to form $[(phen)M]^{+\cdot}$ (Eq. (7)) relative to the barrier heights associated with formation of the metal carbene, $M{=}CH_2$ (Eq. (8)). Bond homolysis is a barrierless process, whereas the formation of $M{=}CH_2$ requires surmounting a transition state, in which a hydrogen from the methyl group translocates to the nitrogen of phenanthroline to form an intermediate, $[(phen)H(M{=}CH_2)]^+$, where the $M{=}CH_2$ moiety is bound coordinatively to the protonated ligand, before dissociation. For every metal, the singlet state has been considered, and for nickel also the triplet state was considered because the triplet precursor ion is 25 kJ mol^{-1} more stable than its singlet state. The respective barriers are compared in a potential energy diagram (Figure 2). The trends are consistent with the experiment: going down group 10, the bond homolysis is disfavored whereas metal carbene formation becomes favored. Furthermore, among the singlet transition states, the one for the formation of $Pt{=}CH_2$ is the lowest. The transition state for the triplet nickel is the lowest, but the energy of the bond homolysis still lies substantially below. However, even if the trends are in agreement with the experiment that bond homolysis occurs for nickel and palladium, but carbene formation is

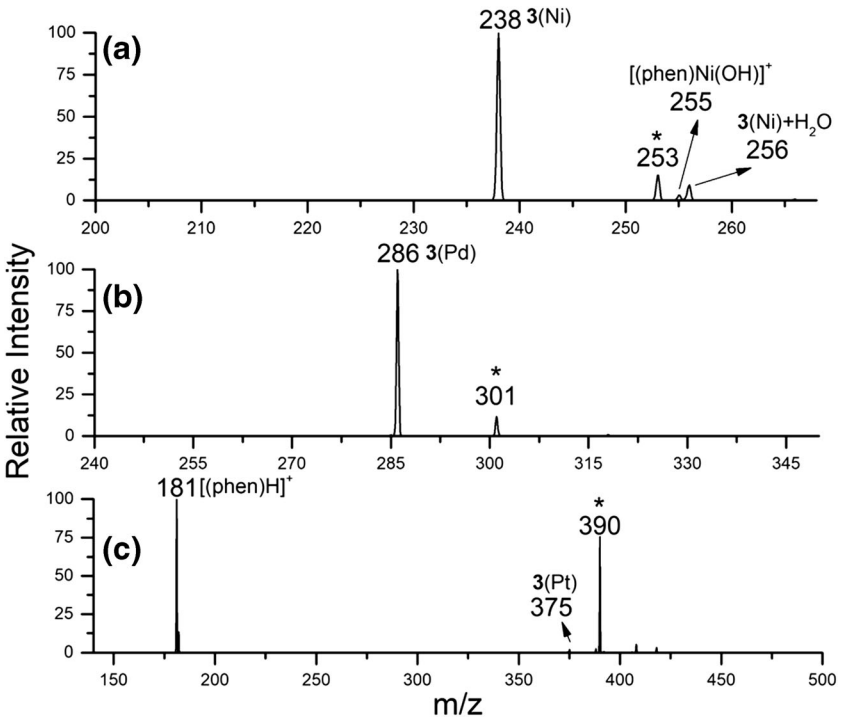

Figure 1. LTQ MS^3 spectra of mass-selected precursor ions, $[(phen)M(CH_3)]^+$, **2**, undergoing CID at a normalized collision energy of 13 for M = Ni, Pd and 20 for M = Pt (arbitrary units) in the linear ion trap: (**a**) M = Ni, (**b**) M = Pd, and (**c**) M = Pt. The mass-selected precursor ions are designated by an asterisk (*)

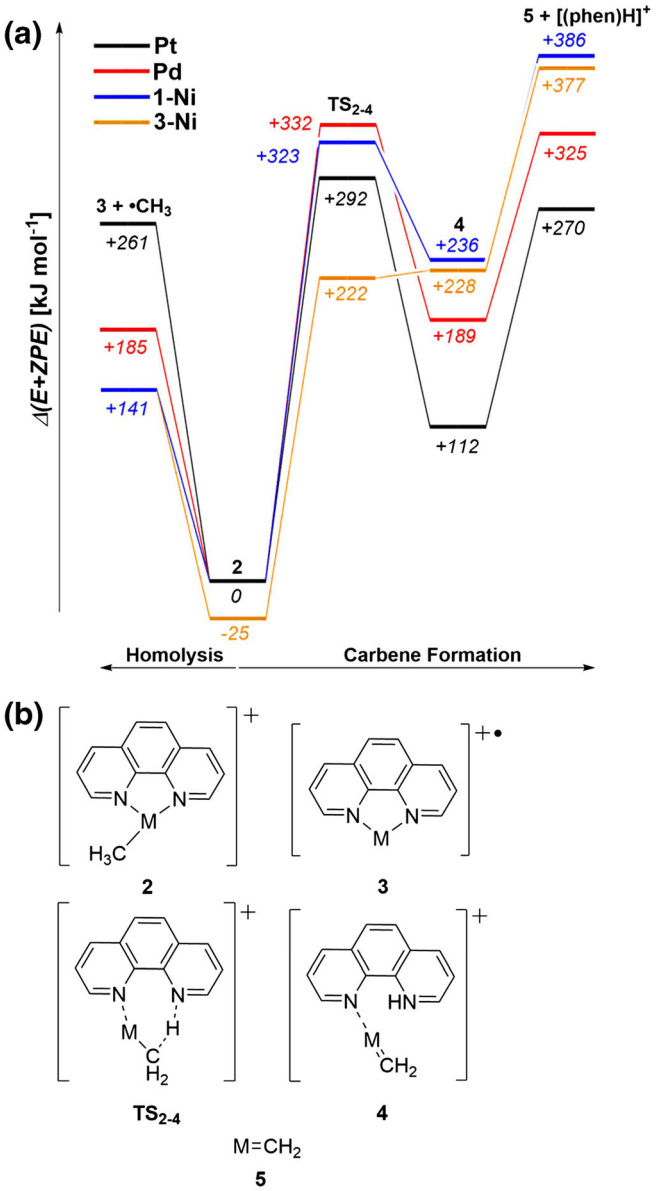

Figure 2. Results of DFT calculations at B3LYP-D3/SDD 6-311G(d) level of theory. (**a**) Plot of the potential energy diagram for both pathways of dissociation of $[(phen)M(CH_3)]^+$ with M = 1-Ni (blue), 3-Ni (orange), Pd (red), and Pt (black); (**b**) structures of key species

preferred for platinum, both the thermodynamics and the kinetics for the competing reaction are not consistent with experiment for the case of platinum. Thus, with the B3LYP-D3/SDD 6-311G(d) level of theory, the bond homolysis requires less energy than forming the transition state and is energetically favored over the formation of protonated phenanthroline and carbene for all the metals. While the B3LYP functional is commonly used, since it generally performs well for geometries and vibrational frequencies; previous detailed benchmarking studies have shown that the B3LYP thermochemistry can often be poorly estimated [78]. Thus, a series of single-point calculations were carried out for platinum with higher levels of theory and different functionals. Single-point energy calculations have been carried out on the structures that were optimized with the B3LYP-D3/SDD 6-311G(d) level of theory with the functionals ωB97X-D3, PWPB95-D3, and DSD-PBEP86-D3 and the basis set def2-TZVPP for all atoms. These functionals were chosen since they have shown to be very robust in past studies, providing better thermochemical estimates [78]. The relevant energetics obtained with these functionals for Pt are given in Table 1 while the potential energy diagrams are given in Fig. S2. With the functionals ωB97X-D3 and PWPB95-D3, the overall energetics for the observed formation of **5** + $[(phen)H]^+$ are thermodynamically favored over bond homolysis to give **3** + $\cdot CH_3$, while for the functional DSD-PBEP86-D3, the energetics are both kinetically and thermodynamically favored for $Pt{=}CH_2$ formation. The best results are given by both double-hybrid functionals PWPB95-D3 and DSD-PBP86-D3, which are expected to perform better than common hybrid DFT functionals [78]. Even at the highest level of theory, the computed surface only loosely aligns with the experimental results since $Pt{=}CH_2$ loss requires a tight transition state and is thus disadvantaged relative to the simple bond cleavage. The problem is likely to be with the energies computed for the simple bond cleavage since Chen has previously noted that theory performs better for the energetics of rearrangement reactions in related ligated Pd cations than for bond homolysis [40].

A key question regarding the $[(phen)M]^{+\cdot}$ metal complexes is whether they are in the +1 oxidation or +2 oxidation state (i.e., where the phen ligand is a redox non-innocent ligand [79]). An examination of the DFT calculated spin density at the metal centers in the $[(phen)M]^{+\cdot}$ metal complexes reveals (Table S1) that they range from 94.7% for M = Ni to 77.8% for M = Pt. This suggests that the complexes can be regarded as being in the +1 oxidation state and that the phen ligand largely behaves as a redox innocent ligand.

IMR of $[(phen)M]^{+\cdot}$ with the Background Gases O_2, N_2, and H_2O

Water and dinitrogen are always present in the ion trap and readily react with the various three-coordinate metal complexes to form adducts (Eqs. (3) and (4)) [34]. The two-coordinate metal complexes, $[(phen)M]^{+\cdot}$, react with background water, dinitrogen, and dioxygen to form adducts (Eq. (6), Figure 3). When M = Ni, mainly water and dioxygen adducts are formed, whereas only a minor peak can be observed for dinitrogen adduct formation. For M = Pd, adduct formation only occurs to a minor degree with water and dioxygen. For M = Pt, adduct formation readily occurs for the three background gases, the water and dinitrogen adduct being favored over dioxygen adduct formation.

Table 1. DFT Calculated Reaction Energetics (in kJ mol^{-1}) for Fragmentation of [(phen)Pt(CH$_3$)]$^+$ via Competing Bond Homolysis Pathway (Giving **3** + ·CH$_3$) and Pt=CH$_2$ Pathway

Level of theory	**3** + ·CH$_3$	**TS$_{2-4}$**	**4**	**5** + [(phen)H]$^+$
M06/SDD 6-31G(d)	+258	+291	+112	+255
B3LYP/SDD 6-31G(d)	+252	+293	+107	+240
B3LYP-D3/SDD 6-31G(d)	+268	+292	+112	+275
B3LYP-D3/SDD 6-311G(d)	+261	+292	+112	+270
ωB97X-D3/def2-TZVPP [a]	+289	+322	+135	+284
PWPB95-D3/def2-TZVPP[a]	+305	+312	+123	+279
DSD-PBEP86–D3/def2-TZVPP[a]	+310	+306	+104	+277

[a]Data is only ΔE since frequency calculations are too expensive for these functionals

The structures and energetics of adduct formation for each metal of the cation [(phen)M]$^{+\cdot}$ have been calculated at the M06/SDD 6-31G(d) level of theory (Figure 3d, Table 2). In the case of water and dinitrogen, an end-on fashioned binding mode is preferred. For dioxygen two stable isomers have been found: one where dioxygen binds in an end-on orientation (η1 hapticity) and one where it binds in a side-on fashion (η2 hapticity), the latter being favored over the former thermodynamically. Overall, the thermodynamics for adduct formation of each background gas with each metal are favorable and follow the order Pt > Ni > Pd, which is consistent with more abundant adduct formation observed in the cases of Pt and Ni (Figure 3c and a) over that of Pd (Figure 3b). The calculated reaction energies for the nitrogen adducts reflect the strength of the orbital overlap, which will be influenced by both the σ and π interactions between the metal center and N_2 [80]. These in turn are affected by factors such as electronegativity and relativistic effects [80, 81]. Thus, nickel is a much better σ-acceptor and π- donor than palladium, while relativistic effects operate on platinum to allow more metal-to-ligand back donation. The η2 binding mode for oxygen for related

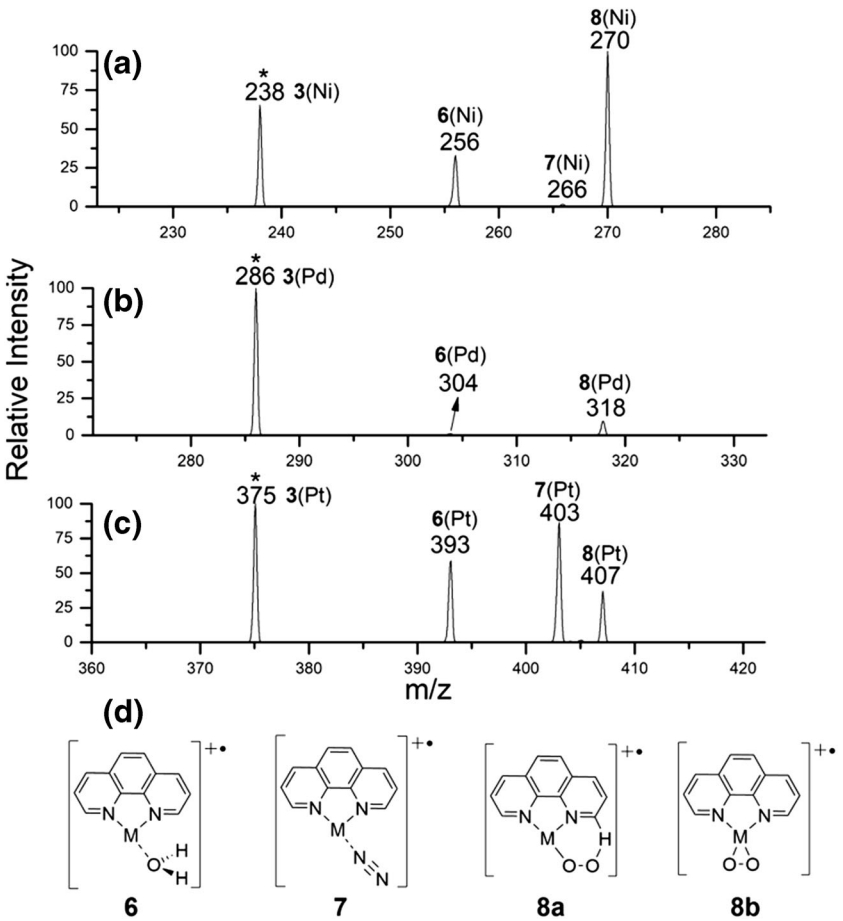

Figure 3. (**a**–**c**) LTQ MS^4 spectra of mass-selected precursor ions, [(phen)M]$^{+\cdot}$, **3**, undergoing IMR at an activation time of 100 ms with background gases present in the linear ion trap: (**a**) M = Ni, (**b**) M = Pd, and (**c**) M = Pt The mass-selected precursor ions are designated by an asterisk (*), (**d**) Structures of key species calculated at the M06/SDD 6-31G(d) level of theory

Table 2. DFT Calculated Reaction Energetics of Forming the Water, Dinitrogen and Dioxygen Adducts of $[(phen)M]^{+\cdot}$ (M = Ni, Pd, Pt) with M06/SDD 6-31G(d) Level of Theory

$[(phen)M]^{+\cdot}$, where M =	H_2O[a]	N_2[a]	O_2 (end-on)[a] **(8a)**	O_2 (side-on)[a] **(8b)**
Ni	−139	−95	−234	−296
Pd	−112	−72	−229	−275
Pt	−137	−115	−269	−348

Reaction of doublet $[(phen)M]^{+\cdot}$ to form doublet products
[a]Reaction energies are $\Delta(E+ZPE)$ in kJ mol^{-1}

ligated Pd(0) complexes has been suggested to arise from oxidation to give a Pd(II) coordinated peroxide [82] and several such complexes have been isolated and structurally characterized via X-ray crystallography [83].

IMR of $[(phen)M]^{+\cdot}$ with Acetone

The metal cations, $[(phen)M]^{+\cdot}$, form the adducts, $[(phen)M(OC(CH_3)_2)]^{+\cdot}$, with acetone in IMR (Eq. (9), Figure 4). In the case of Pt, a minor ion is observed at *m/z*

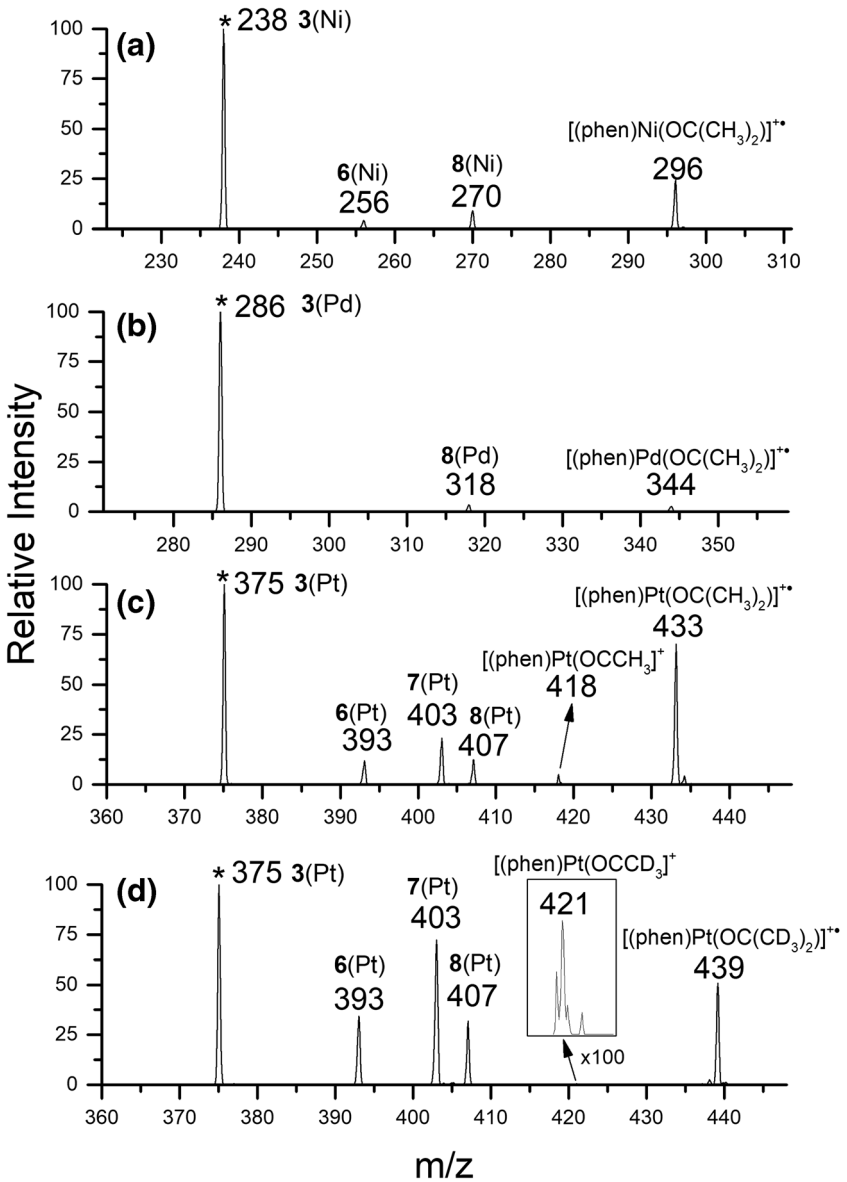

Figure 4. LTQ MS^4 spectra of mass-selected precursor ions, $[(phen)M]^{+\cdot}$, undergoing IMR at an activation time of 100 MS with acetone (**a**–**c**) and acetone-d_6 (**d**) in the linear ion trap: (**a**) M = Ni, (**b**) M = Pd, and (**c**–**d**) M = Pt. The mass-selected precursor ions are designated by an asterisk (*)

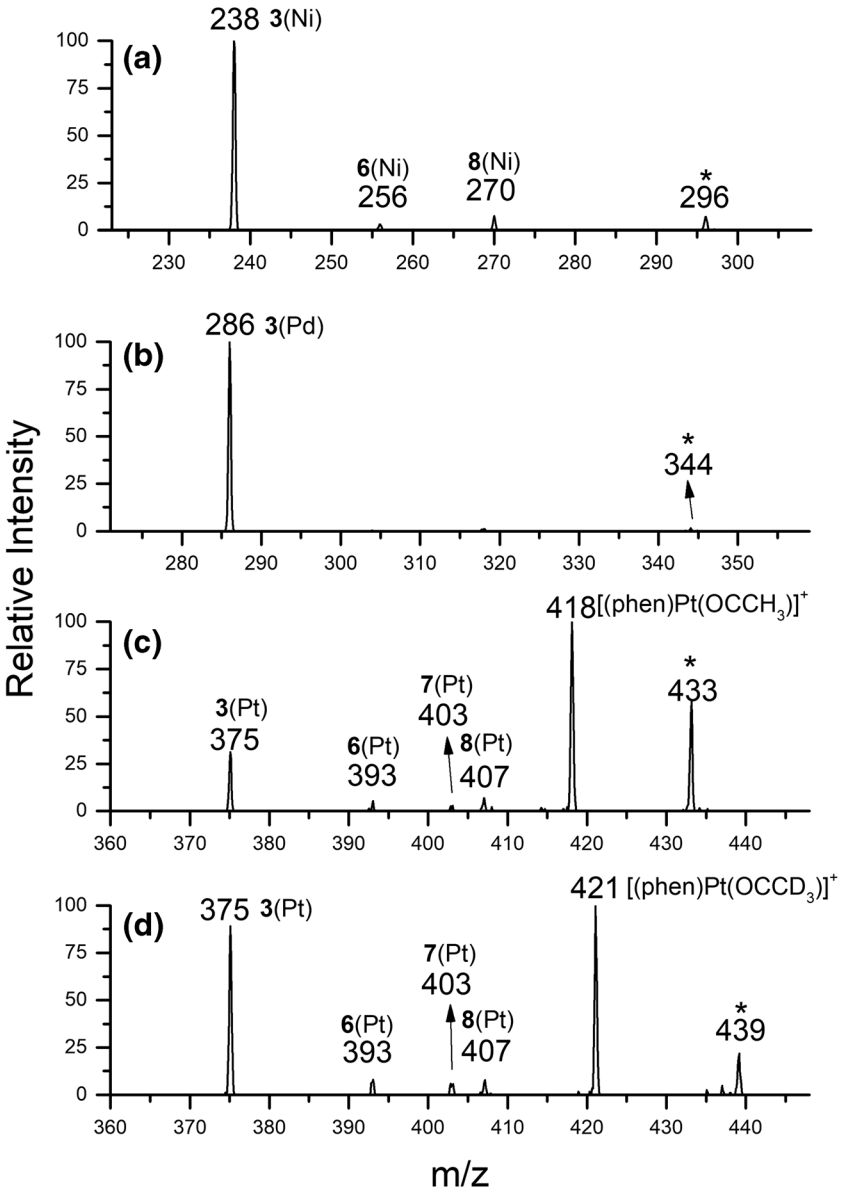

Figure 5. LTQ MS^5 spectra of mass-selected precursor ions, $[(phen)M(OC(CH_3)_2)]^{+\bullet}$ undergoing CID at a normalized collision energy of 20 (arbitrary units) in the linear ion trap: (**a**) M = Ni, (**b**) M = Pd, and (**c**–**d**) M = Pt. The mass-selected precursor ions are designated by an asterisk (*)

418, which corresponds to a loss of a methyl radical from the acetone adduct to form the coordinated acyl anion $[(phen)Pt(OCCH_3)]^+$ (Eq. (10)). The analogous peak is observed as a minor peak in the case of acetone-d_6, likely due to the operation of a secondary kinetic isotope effect for the formation of $[(phen)Pt(OCCD_3)]^+$ [84]. The observed reactivity for the ligated metal cations, $[(phen)M]^{+\cdot}$ contrast to the behavior of the bare metal ions, which activate the C–C bond of acetone to produce ethane as the major product (Eq. (12)) and CO as the minor product (Eq. (12)) [42–46].

$$[(phen)M]^{+\bullet} + OC(CX_3)_2 \rightarrow [(phen)M(OC(CX_3)_2)]^{+\bullet} \quad (M = Ni, Pd, Pt) \tag{9}$$

$$[(phen)Pt]^{+\bullet} + OC(CX_3)_2 \rightarrow [(phen)Pt(OCCX_3)]^{+} + {\bullet}CX_3 \tag{10}$$

where X = H or D

$$M^{+\bullet} + OC(CH_3)_2 \rightarrow \left[M(CO)\right]^{+\bullet} + C_2H_6 \quad (M = Ni, Pd) \tag{11}$$

$$\rightarrow \left[M(CH_3)_2\right]^{+\bullet} + CO \quad (M = Ni, Pd) \tag{12}$$

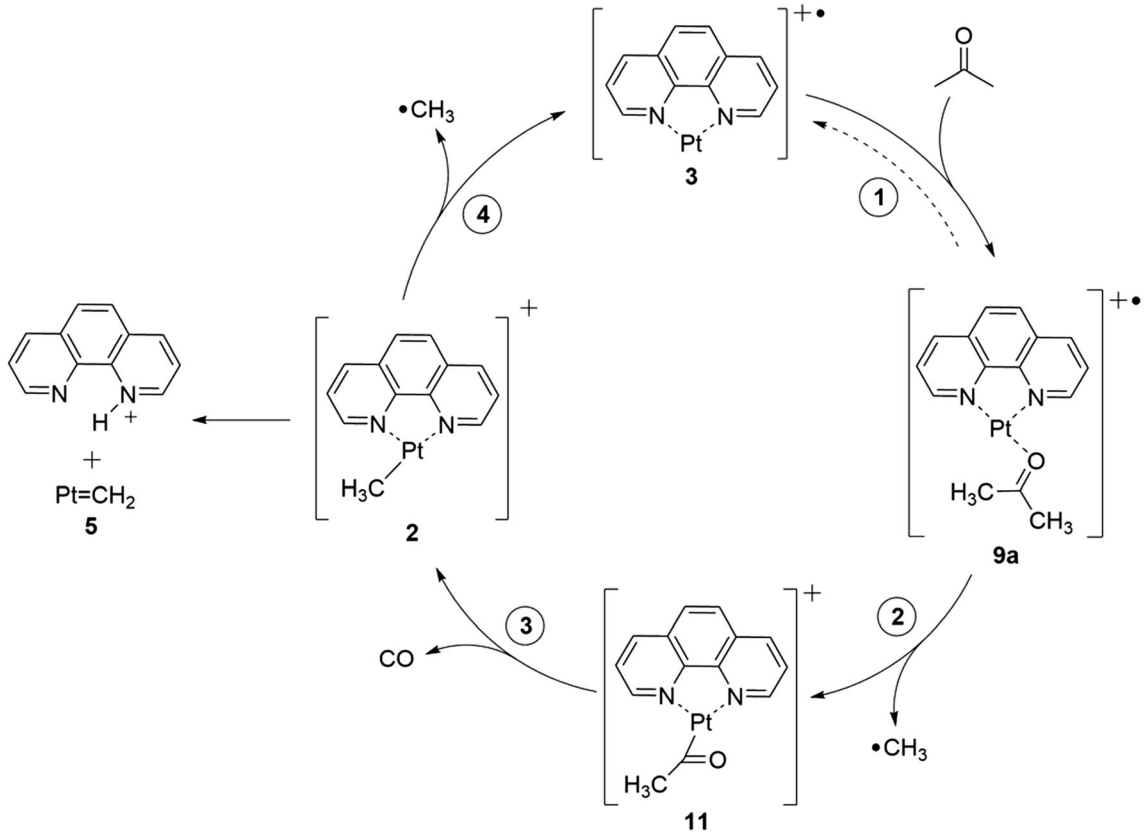

Scheme 1. Catalytic cycle for the decomposition of acetone mediated by $[(phen)Pt]^{+\bullet}$

Upon CID, the acetone adducts dissociate to regenerate $[(phen)M]^{+\bullet}$ in the case of M = Ni, Pd (Eq. (13)). For M = Pt, the dissociation is only a minor pathway compared to the loss of a methyl radical to form the acyl complex $[(phen)Pt(OCCH_3)]^+$ (Eq. (14), Figure 5, *m/z* 418). The loss of methyl radical (15 Da) was confirmed by deuterium labeling experiments with fully deuterated acetone, where a mass loss of 18 Da was observed. The differences in branching ratios for $OC(CH_3)_2$ (BR Eq. (13) = 19.5%) versus $OC(CD_3)_2$ (BR Eq. (13) = 42.5%) and for $\cdot CH_3$ (BR Eq. (14) = 70.2%) versus $\cdot CD_3$ (BR Eq. (14) = 45.6%) losses suggest that a secondary isotope effect (k_H/k_D) operates for the C–C bond cleavage step associated with methyl radical loss. An estimate of k_H/k_D of 1.5 is derived from BR($\cdot CH_3$ loss, Eq. (14))/BR($\cdot CD_3$ loss, Eq. (14)) [84]. This is much smaller than the k_H/k_D of 5.5 measured for the loss of ethane from the $[Ni(OC(CH_3)_2)]^{+\cdot}$ complex, which was suggested to arise from a rate-limiting step of C–C bond coupling rather than C–C bond activation [46].

$$[(phen)M(OC(CX_3)_2)]^{+\bullet} \rightarrow [(phen)M]^{+\bullet} + OC(CX_3)_2 \quad (M = Ni, Pd) \tag{13}$$

$$[(phen)Pt(OC(CX_3)_2)]^{+\bullet} \rightarrow [(phen)Pt(OCCX_3)]^{+} + \bullet CX_3 \tag{14}$$

where X = H or D

Upon further CID, the acyl complex $[(phen)Pt(OCCH_3)]^+$ (*m/z* 418) loses CO to regenerate the three-coordinate methyl complex $[(phen)Pt(CH_3)]^+$ (Eq. (15), *m/z* 390). In the deuterium labeling experiments, the same complex was generated with a fully deuterated methyl ligand (Fig. S3). Thus, in contrast to the nickel and palladium complexes, $[(phen)Pt]^{+\cdot}$ formally catalyzes the decomposition of acetone into CO and two methyl radicals (Eq. (16), Scheme 1). Although photolysis or thermolysis of acetone gives a range

Table 3. DFT Calculated Reaction Energetics of the Catalytic Cycle of the Decomposition of Acetone Mediated by $[(phen)Pt]^{+\cdot}$ with M06/SDD 6-31G(d) Level of Theory

Isomer formed	Step 1 (formation of adducts **9a**–**9c**, Eq. (9))[a]	Step 2 (Acyl formation, Eq. (11))[a]	Step 3[a]	Step 4[a]
Isomer **a**	−177	+185	+155	+258
Isomer **b**	−169	+202	/	/
Isomer **c**	−91	/	/	/

[a]Reaction energies are $\Delta(E+ZPE)$ in kJ mol^{-1}

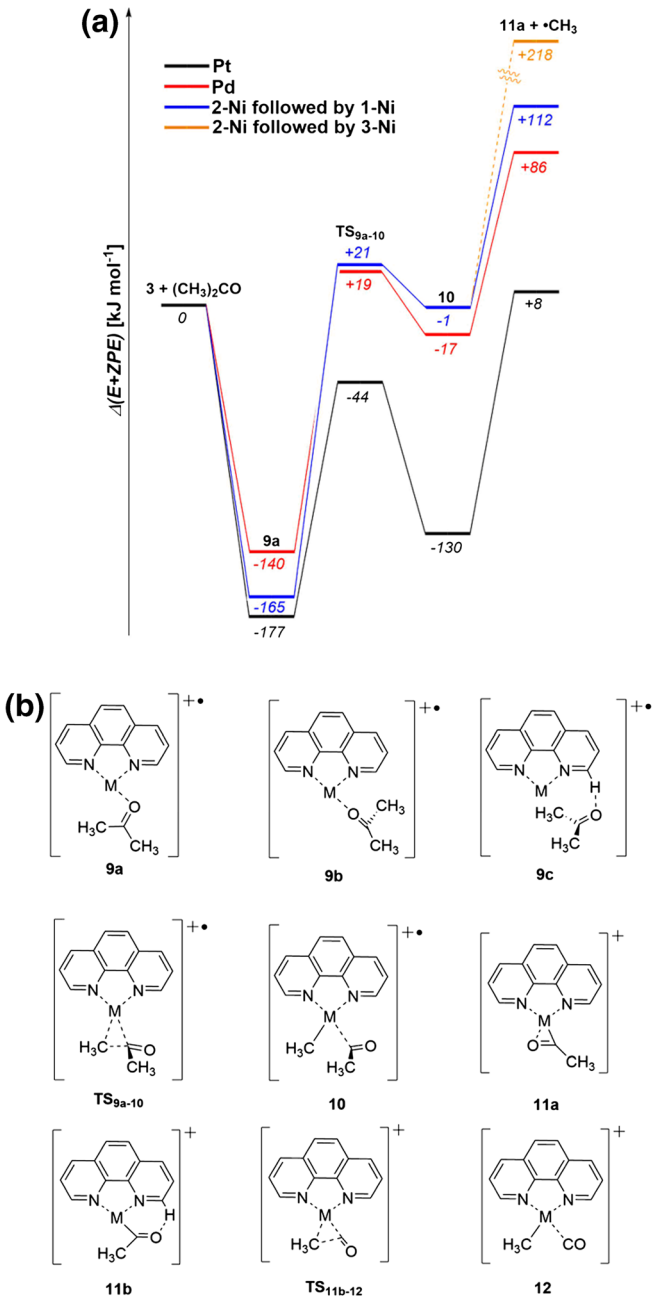

Figure 6. DFT calculations at M06/SDD 6-31G(d) level of theory. (**a**) Plot of the potential energy diagram for acetone adduct formation and subsequent methyl loss for $[(phen)M(CH_3)]^+$ with M = 2-Ni (followed by 1-Ni (to give singlet product: blue), 3-Ni (to give triplet product: orange), Pd (red) and Pt (black); (**b**) structures of key species

of products, C–C bond homolysis to give methyl radicals is a key channel [85, 86].

$$[(phen)Pt(OCCH_3)]^+ \rightarrow [(phen)Pt(CH_3)]^+ + CO \quad (15)$$

$$(CH_3)_2CO \rightarrow CO + 2{\bullet}CH_3 \quad (16)$$

An examination of the catalytic cycle (Scheme 1) reveals that it suffers from the off cycle Pt=CH_2 loss (Eq. (8)) being the dominant pathway, with the regeneration of the catalyst **3** being only a minor product in step 4. Nonetheless, DFT calculations were carried out to examine the energetics associated with all steps and the data is summarized in Table 3. Adduct formation is exothermic for step 1, consistent with the observation that this reaction occurs under the IMR conditions. Three different adducts (**9a**–**9c**) were located (Figure 6b). For step 2 of the cycle, the transition state $\mathbf{TS_{9a\text{-}10}}$ for activating the C–C bond of acetone to form a methyl acyl intermediate $[(phen)Pt(CH_3)(OCCH_3)]^+$ (**10**) is favored over the dissociation of the adduct to give **3** (Figure 6, black surface). For the Pd (red surface) and the Ni complexes (which can give either the singlet (blue surface) or triplet (orange surface)), however, the formation of an acyl complex is disfavored both thermodynamically and kinetically, as the energies of the transition state and the acyl complex are higher than the energy needed for the dissociation of the adduct. The formation of the acyl complex **11** requires energy, which is delivered upon CID. However, the dissociation of the intermediate adduct(s) **9a-c** via $\mathbf{TS_{9a\text{-}10}}$ requires less energy than the formation of the acyl complex. The energy difference of 8 kJ mol^{-1} lies within the error of the functional used [78].

The decarbonylation of **11** in step 3 to regenerate the methyl complex, $[(phen)Pt(CH_3)]^+$(**2**), and carbon monoxide requires 139 kJ mol^{-1} (Fig. S4), as found for the related decarbonylation of the bidentate enolate complex $[(phen)Pt((OC(CH_2)CH_3)]^+$ [47]. The transition state $\mathbf{TS_{11b\text{-}12}}$ lies only 1 kJ mol^{-1} above the acyl complex **11b**, while the intermediate **12**, in which CO is still coordinatively bound to the metal center, lies below **11b** (− 102 kJ mol^{-1}). Finally, the energetics associated with regeneration of the catalyst, **3**, has already been discussed in detail in "Bond Homolysis vs. Carbene Formation."

IMR with Allyl Iodide

The IMR spectra of $[(phen)M]^{+\bullet}$ with allyl iodide are given in Figure 7. For all three metals, Ni, Pd, and Pt the formation of an allyl complex via allyl abstraction are observed (Eq. (17)). A previous report noted that $[(phen)Ni]^{+\bullet}$ reacts via allyl abstraction as the major reaction together with the formation of the minor product due to the addition of allyl iodide [41]. For M = Pt two further products could be observed: the iodo complex $[(phen)Pt(I)]^+$ and the diiodoallyl complex $[(phen)Pt(I)_2(CH_2CHCH_2)]^+$ (Eqs. (18) and (19)). The iodo complex also reacts with background gases to form the respective adducts (Eq. (20)).

$$[(phen)M]^{+\bullet} \quad CH_2CHCH_2I \rightarrow [(phen)M(CH_2CHCH_2)]^+ + {\bullet}I \quad (M = Ni, Pd, Pt) \quad (17)$$

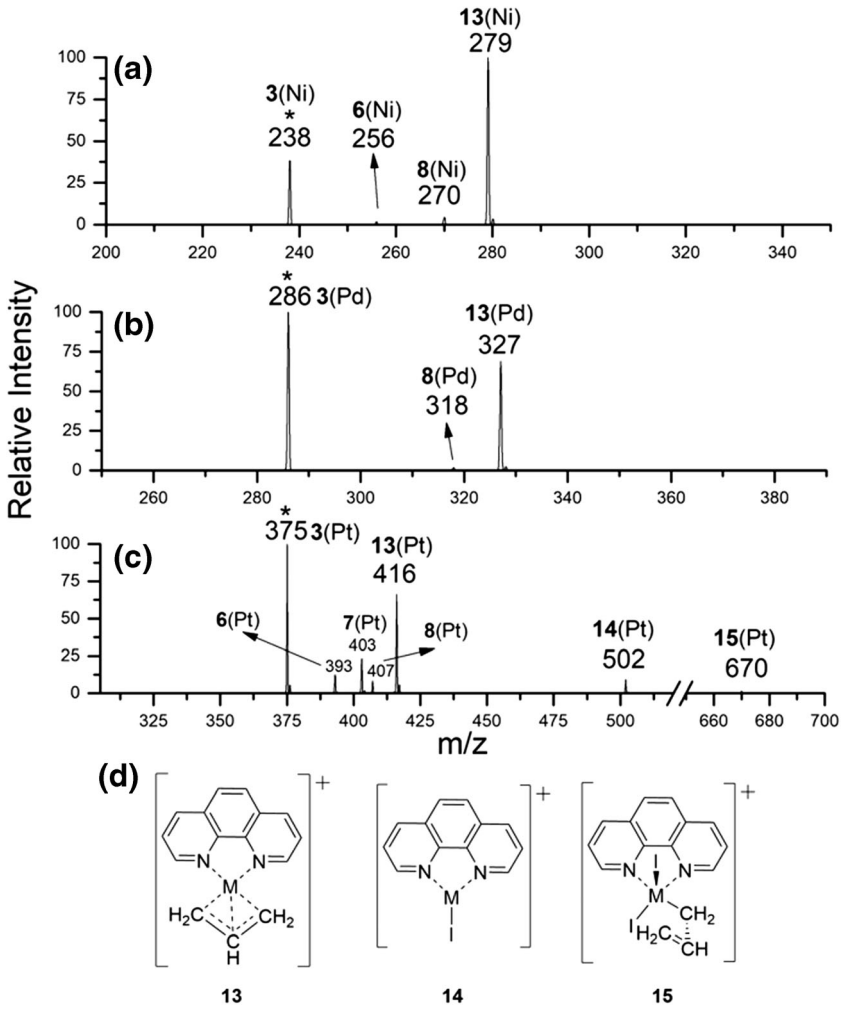

Figure 7. (**a**–**c**) LTQ MS^4 spectra of mass-selected precursor ions, $[(phen)M]^{+\bullet}$, undergoing IMR at an activation time of 30 ms with allyl iodide in the linear ion trap (infusion rate 50 μL/h): (**a**) M = Ni, (**b**) M = Pd, and (**c**) M = Pt. The mass-selected precursor ions are designated by an asterisk (*); (**d**) structures of key species

$$[(phen)Pt]^{+\bullet} \quad CH_2CHCH_2I \rightarrow [(phen)Pt(I)]^+ + \bullet CH_2CHCH_2 \tag{18}$$

$$[(phen)Pt(I)]^+ + CH_2CHCH_2I \rightarrow [(phen)Pt(I)_2(CH_2CHCH_2)]^+ \tag{19}$$

$$[(phen)Pt(I)]^+ + L \rightarrow [(phen)Pt(I)(L)]^+ \tag{20}$$

The energetics of the observed reactions have been calculated (Figure 7d, Table 4). The energetics of the three reactions giving **13**, **14**, and **15** as singlets become more favorable going down group 10. The allyl abstraction is thermodynamically favored for each metal, whereas the iodine abstraction is only favored for

Table 4. DFT Calculated Reaction Energetics for the Formation of Products **13**–**15** in the Reactions of $[(phen)M]^{+\cdot}$ with Allyl Iodide with M06/SDD 6-31G(d) Level of Theory

Spin state of product	**13** via Eq. (17)[c]	**14** via Eq. (18)[c]	**15** via Eq. (19)[c]
1-Ni[a]	−64	+42	−19
3-Ni[b]	+58 [d]	−3	−52
1-Pd[a]	−109	+25	−89
1-Pt[a]	−202	−69	−217

[a]Reaction of doublet $[(phen)M]^{+\cdot}$ to form metal product ion in singlet state
[b]Reaction of doublet $[(phen)M]^{+\cdot}$ to form metal product ion in triplet state
[c]Reaction energies are $\Delta(E+ZPE)$ in kJ mol^{-1}
[d]Attempted optimization of a triplet structure in M06 led to spin annihilation but was successfully carried out in B3LYP. The energetics were then obtained via single-point energy calculations of this structure with M06/SDD 6-31G(d) level of theory

platinum. The formation of $[(phen)M(I)_2(CH_2CHCH_2)]^+$ is favored for each metal, but can only be observed for platinum. This is consistent with the calculated thermochemistry for the stepwise formation of $[(phen)M(I)_2(CH_2CHCH_2)]^+$, which requires the formation of $[(phen)M(I)]^+$, which is only favored for platinum. Since the ground state of nickel complexes can vary, we also calculated the thermochemistry for the formation of the triplet states of **13**, **14**, and **15**. Just as the parent three-coordinate complex $[(phen)Ni(CH_3)]^+$ has been shown to be more stable in the triplet state [47], so too are the triplets of the nickel complexes of **14** and **15**. For **13**, however, the singlet state in which the allyl ligand adopts a η^3 binding mode is more stable than the triplet in which allyl ligand binds in a η^1 fashion. Similar differences in the singlet versus triplet stabilities have been calculated for the formation of $[(phen)Ni(CH_2CHCH_2)]^+$ and $[(phen)Ni(Br)]^+$ in the reactions of allyl bromide with $[(phen)Ni]^{+\cdot}$ [41]. Overall, the theoretical results are consistent with the experiments: only singlet formation is expected to be kinetically viable since triplet formation requires the participation of an electron from a filled d orbital on the reactant ion. Formation of singlet **13** is exothermic in all cases and is observed for all metals (Figure 7). Formation of singlet **14**, the precursor to formation of singlet **15**, is only exothermic for Pt, which is why formation of **14** (via Eq. (18)) and **15** (via Eq. (19)) is only observed in the IMR of $[(phen)Pt]^{+\cdot}$ (Figure 7c).

Conclusion

Gas-phase studies allow a systematic evaluation of the role of ligand and metal oxidation state on reactivity. By studying all members of a group, it is possible to relate changes in reactivity to electronic effects. In previous work, we have shown that only $[(phen)Pt(CH_3)]^+$ reacts with acetone to form the enolate $[(phen)Pt(OC(CH_2)CH_3)]^+$ [47]. Here, we have shown that MS^n experiments in a linear ion trap mass spectrometer readily yield the ligated group 10 metal complexes $[(phen)M]^{+\cdot}$ in the formal oxidation state of +1, thereby allowing their bimolecular reactivity to be explored. Of all the metals, Pt stands out once again for two of the reactions studied. In the fragmentation of $[(phen)Pt(CH_3)]^+$, the desired bond homolysis is only a minor pathway, while the loss of the neutral carbene $Pt{=}CH_2$ dominates. The acetone adduct $[(phen)Pt(OC(CH_3)_2)]^{+\cdot}$ fragments via methyl radical loss to form the coordinated acyl complex, $[(phen)Pt(OCCH_3)]^+$, a reaction that is unique for Pt. It will be interesting to explore the gas-phase formation and reactivity of other $[(L)M]^{+\cdot}$ complexes in which the ligand, L, exerts different geometrical and electronic effects to 1,10-phenanthroline. One class of ligands that would be particularly interesting are phosphine-based ligands. Previous studies suggest that alternative "synthetic" strategies to CID of carboxylate complexes are required since decarbonylation rather than decarboxylation occurs for $[CH_3CO_2Pd((PPh_2)_2CH_2)]^+$ [87]. Given the widespread success of photoactivated C–I bond homolysis [88] and that Pd-azide bonds in Pd(II) complexes are known to undergo photoactivated bond homolysis [89], we are exploring whether related M–X photoactivated bond homolysis could be used to prepare $[(L)M]^{+\cdot}$ from suitable precursors.

Acknowledgements

We thank the Australian Research Council for financial support DP180101187 (to RAJO and AJC). The authors gratefully acknowledge the generous allocation of computing time from the University of Tasmania and the National Computing Infrastructure (fz2). We are particularly thankful to the DAAD (ISAP program) for funding an exchange program between the Schools of Chemistry of Humboldt-Universität zu Berlin and The University of Melbourne. KG is grateful to the "Fondation Félix Chomé" for the "Bourse Chomé-Bastian" scholarship.

References

1. Johansson Seechurn, C.C.C., Kitching, M.O., Colacot, T.J., Snieckus, V.: Palladium-catalyzed cross-coupling: a historical contextual perspective to the 2010 Nobel Prize. Angew. Chem. Int. Ed. **51**, 5062–5085 (2012)
2. Bonney, K.J., Schoenebeck, F.: Experiment and computation: a combined approach to study the reactivity of palladium complexes in oxidation states 0 to IV. Chem. Soc. Rev. **43**, 6609–6638 (2014)
3. Ananikov, V.P., Zelinsky, N.D.: Nickel: the "spirited horse" of transition metal catalysis. ACS Catal. **5**, 1964–1971 (2015)
4. Lin, C.-Y., Power, P.P.: Complexes of Ni(I): a "rare" oxidation state of growing importance. Chem. Soc. Rev. **46**, 5347–5399 (2017)
5. Zimmermann, P., Limberg, C.: Activation of small molecules at nickel(I) moieties. J. Am. Chem. Soc. **139**, 4233–4242 (2017)
6. Balch, A.L.: Odd oxidation states of palladium and platinum. Comments Inorg. Chem. **3**, 51–67 (1984)
7. Simpson, Q., Sinclair, M.J.G., Lupton, D.W., Chaplin, A.B., Hooper, J.F.: Oxidative cross-coupling of boron and antimony nucleophiles via palladium(I). Org. Lett. **20**, 5537–5540 (2018)
8. Zuo, Z., Ahneman, D.T., Chu, L., Terrett, J.A., Doyle, A.G., MacMillan, D.W.C.: Dual catalysis. Merging photoredox with nickel catalysis: coupling of α-carboxyl sp^3-carbons with aryl halides. Science. **345**, 437–440 (2014)
9. Tellis, J.C., Kelly, C.B., Primer, D.N., Jouffroy, M., Patel, N.R., Molander, G.A.: Single-electron transmetalation via photoredox/nickel dual catalysis: unlocking a new paradigm for sp^3-sp^2 cross-coupling. Acc. Chem. Res. **49**, 1429–1439 (2016)
10. Matsui, J.K., Lang, S.B., Heitz, D.R., Molander, G.A.: Photoredox-mediated routes to radicals: the value of catalytic radical generation in synthetic methods development. ACS Catal. **7**, 2563–2575 (2017)
11. Menges, F.S., Craig, S.M., Tötsch, N., Bloomfield, A., Ghosh, S., Krüger, H.J., Johnson, M.A.: Capture of CO_2 by a cationic nickel(I) complex in the gas phase and characterization of the bound, activated CO_2 molecule by cryogenic ion vibrational predissociation spectroscopy. Angew. Chem. Int. Ed. **55**, 1282–1285 (2016)
12. Craig, S.M., Menges, F.S., Johnson, M.A.: Application of gas phase cryogenic vibrational spectroscopy to characterize the CO_2, CO, N_2 and N_2O interactions with the open coordination site on a Ni(I) macrocycle using dual cryogenic ion traps. J. Mol. Spectrosc. **332**, 117–123 (2017)
13. Yalcin, T., Wang, J., Wen, D., Harrison, A.G.: C-C and C-H bond activation in the fragmentation of the $[M + Ni]^+$ adducts of aliphatic amino acids. J. Am. Soc. Mass Spectrom. **8**, 749–755 (1997)
14. Mó, O., Yáñez, M., Salpin, J.-Y., Tortajada, J.: Thermochemistry, bonding, and reactivity of Ni^+ and Ni^{2+} in the gas phase. Mass Spectrom. Rev. **26**, 474–516 (2007)
15. O'Hair, R.A.J.: Mass spectrometry based studies of gas phase metal catalyzed reactions. Int. J. Mass Spectrom. **377**, 121–129 (2015)
16. Eller, K., Schwarz, H.: Organometallic chemistry in the gas phase. Chem. Rev. **91**, 1121–1177 (1991)

17. Böhme, D.K., Schwarz, H.: Gas-phase catalysis by atomic and cluster metal ions: the ultimate single-site catalysts. Angew. Chem. Int. Ed. **44**, 2336–2354 (2005)
18. Schwarz, H.: Ménage-à-trois: single-atom catalysis, mass spectrometry, and computational chemistry. Catal. Sci. Technol. **7**, 4302–4314 (2017)
19. Schwarz, H.: Chemistry with methane: concepts rather than recipes. Angew. Chem. Int. Ed. **50**, 10096–10115 (2011)
20. Schwarz, H.: How and why do cluster size, charge state, and ligands affect the course of metal-mediated gas-phase activation of methane? Isr. J. Chem. **54**, 1413–1431 (2014)
21. Schwarz, H.: Remote functionalization of C-H and C-C bonds by "naked" transition-metal ions (Cosi Fan Tutte). Acc. Chem. Res. **22**, 282–287 (1989)
22. Schröder, D., Shaik, S., Schwarz, H.: Two-state reactivity as a new concept in organometallic chemistry. Acc. Chem. Res. **33**, 139–145 (2000)
23. Vikse, K.L., McIndoe, J.S.: Mechanistic insights from mass spectrometry: examination of the elementary steps of catalytic reactions in the gas phase. Pure Appl. Chem. **87**, 361–377 (2015)
24. Vikse, K.L., Ahmadi, Z., McIndoe, J.S.: The application of electrospray ionization mass spectrometry to homogeneous catalysis. Coord. Chem. Rev. **279**, 96–114 (2014)
25. Heinemann, C., Wesendrup, R., Schwarz, H.: Pt^+-mediated activation of methane: theory and experiment. Chem. Phys. Lett. **239**, 75–83 (1995)
26. Božović, A., Feil, S., Koyanagi, G.K., Viggiano, A.A., Zhang, X., Schlangen, M., Schwarz, H., Bohme, D.K.: Conversion of methane to methanol: nickel, palladium, and platinum (d9) cations as catalysts for the oxidation of methane by ozone at room temperature. Chem. Eur. J. **16**, 11605–11610 (2010)
27. Georgiadis, R., Fisher, E.R., Armentrout, P.B.: Neutral and ionic metal-hydrogen and metal-carbon bond energies: reactions of cobalt, nickel, and copper with ethane, propane, methylpropane, and dimethylpropane. J. Am. Chem. Soc. **111**, 4251–4262 (1989)
28. van Koppen, P.A.M., Bowers, M.T., Fisher, E.R., Armentrout, P.B.: Relative energetics of C-H and C-C Bond activation of alkanes: reactions of Ni^+ and Fe^+ with propane on the lowest energy (adiabatic) potential energy surfaces. J. Am. Chem. Soc. **116**, 3780–3791 (1994)
29. Zhang, X.-G., Liyanage, R., Armentrout, P.B.: Potential energy surface for activation of methane by Pt^+: a combined guided ion beam and DFT study. J. Am. Chem. Soc. **123**, 5563–5575 (2001)
30. Mansell, A., Theis, Z., Gutierrez, M.G., Faza, O.N., Lopez, C.S., Bellert, D.J.: Submerged barriers in the Ni^+ assisted decomposition of propionaldehyde. J. Phys. Chem. A. **120**, 2275–2284 (2016)
31. Robinson, P.S.D., Khairallah, G.N., da Silva, G., Lioe, H., O'Hair, R.A.J.: Gold-mediated C-I bond activation of iodobenzene. Angew. Chem. Int. Ed. **51**, 3812–3817 (2012)
32. Luman, C.R., Castellano, F.N.: Phenanthroline ligands. In: McCleverty, J.A., Meyer, T.J. (eds.) Comprehensive coordination chemistry II, pp. 25–39. Elsevier, Amsterdam (2003)
33. O'Hair, R.A.J., Rijs, N.J.: Gas phase studies of the Pesci decarboxylation reaction: synthesis, structure, and unimolecular and bimolecular reactivity of organometallic ions. Acc. Chem. Res. **48**, 329–340 (2015)
34. Woolley, M.J., Khairallah, G.N., Donnelly, P.S., O'Hair, R.A.J.: Nitrogen adduction by three coordinate group 10 organometallic cations: platinum is favoured over nickel and palladium. Rapid Commun. Mass Spectrom. **25**, 2083–2088 (2011)
35. Woolley, M., Ariafard, A., Khairallah, G.N., Kwan, K.H.-Y., Donnelly, P.S., White, J.M., Canty, A.J., Yates, B.F., O'Hair, R.A.J.: Decarboxylative-coupling of allyl acetate catalyzed by group 10 organometallics, $[(phen)M(CH_3)]^+$. J. Org. Chem. **79**, 12056–12069 (2014)
36. Woolley, M.J., Khairallah, G.N., da Silva, G., Donnelly, P.S., Yates, B.F., O'Hair, R.A.J.: Role of the metal, ligand, and alkyl/aryl group in the hydrolysis reactions of group 10 organometallic cations $[(L)M(R)]^+$. Organometallics. **32**, 6931–6944 (2013)
37. Woolley, M., Khairallah, G.N., da Silva, G., Donnelly, P.S., O'Hair, R.A.J.: Direct versus water-mediated protodecarboxylation of acetic acid catalyzed by group 10 carboxylates, $[(phen)M(O_2CCH_3)]^+$. Organometallics. **33**, 5185–5197 (2014)
38. Noor, A., Li, J., Khairallah, G.N., Li, Z., Ghari, H., Canty, A.J., Ariafard, A., Donnelly, P.S., O'Hair, R.A.J.: A one-pot route to thioamides discovered by gas-phase studies: palladium-mediated CO_2 extrusion followed by insertion of isothiocyanates. Chem. Commun. **53**, 3854–3857 (2017)
39. Yang, Y., Noor, A., Canty, A.J., Ariafard, A., Donnelly, P.S., O'Hair, R.A.J.: Synthesis of amidines by palladium-mediated CO_2 extrusion followed by insertion of carbodiimides: translating mechanistic studies to develop a one-pot method. Organometallics. **38**, 424–435 (2019)
40. Zhugralin, A.R., Kobylianskii, I.J., Chen, P.: Experimental gas-phase and in silico investigation of β-methyl elimination from cationic palladium alkyl species. Organometallics. **34**, 1301–1306 (2015)
41. Parker, M.L., Gronert, S.: Investigating reduced metal species via sequential ion/ion and ion/molecule reactions: the reactions of transition metal phenanthrolines with allyl iodide. Int. J. Mass Spectrom. **418**, 73–78 (2017)
42. Halle, L.F., Crowe, W.E., Armentrout, P.B., Beauchamp, J.L.: Reactions of atomic cobalt ions with aldehydes and ketones. Observation of decarbonylation processes leading to formation of metal alkyls and metallacycles in the gas phase. Organometallics. **3**, 1694–1706 (1984)
43. Tolbert, M.A., Mandich, M.L., Halle, L.F., Beauchamp, J.L.: Activation of alkanes by ruthenium, rhodium, and palladium ions in the gas phase: striking differences in reactivity of first- and second-row metal ions. J. Am. Chem. Soc. **108**, 5675–5683 (1986)
44. Carpenter, C.J., van Koppen, P.A.M., Bowers, M.T.: Details of potential energy surfaces involving C-C bond activation: reactions of Fe^+, Co^+, and Ni^+ with acetone. J. Am. Chem. Soc. **117**, 10976–10985 (1995)
45. Chen, X., Guo, W., Zhao, L., Fu, Q.: Theoretical survey of the potential energy surface of Ni^+ + acetone reaction. Chem. Phys. Lett. **432**, 27–32 (2006)
46. Dee, S.J., Castleberry, V.A., Villarroel, O.J., Laboren, I.E., Frey, S.E., Ashley, D., Bellert, D.J.: Rate-limiting step in the low-energy unimolecular decomposition reaction of $Ni^{+\bullet}$ acetone into Ni^+CO + ethane. J. Phys. Chem. A. **113**, 14074–14080 (2009)
47. Greis, K., Canty, A.J., O'Hair, R.A.J.: Gas-phase reactions of the group 10 organometallic cations, $[(phen)M(CH_3)]^+$ with acetone: only platinum promotes a catalytic cycle via the enolate $[(phen)Pt(OC(CH_2)CH_3)]^+$. Z. Phys. Chem. (in press). https://doi.org/10.1515/zpch-2018-135571
48. Thum, C.C.L., Khairallah, G.N., O'Hair, R.A.J.: Gas-phase formation of the Gomberg-Bachmann magnesium ketyl. Angew. Chem. Int. Ed. **47**, 9118–9121 (2008)
49. Vikse, K.L., Zavras, A., Thomas, T.H., Ariafard, A., Khairallah, G.N., Canty, A.J., Yates, B.F., O'Hair, R.A.J.: Prying open a reactive site for allylic arylation by phosphine-ligated geminally diaurated aryl gold complexes. Organometallics. **34**, 3255–3263 (2015)
50. Rijs, N.J., Yoshikai, N., Nakamura, E., O'Hair, R.A.J.: Gas-phase reactivity of group 11 dimethylmetallates with allyl iodide. J. Am. Chem. Soc. **134**, 2569–2580 (2012)
51. Price, J.H., Williamson, A.N., Schramm, R.F., Wayland, B.B.: Palladium(II) and platinum(II) alkyl sulfoxide complexes. Examples of sulfur-bonded, mixed sulfur- and oxygen-bonded, and totally oxygen-bonded complexes. Inorg. Chem. **11**, 1280–1284 (1972)
52. Fanizzi, F.P., Natile, G., Lanfranchi, M., Tiripicchio, A., Laschi, F., Zanello, P.: Steric crowding and redox reactivity in platinum(II) and platinum(IV) complexes containing substituted 1,10-phenanthrolines. Inorg. Chem. **35**, 3173–3182 (1996)
53. Soro, B., Stoccoro, S., Minghetti, G., Zucca, A., Cinellu, M.A., Gladiali, S., Manassero, M., Sansoni, M.: Synthesis of the first C-2 cyclopalladated derivatives of 1,3-Bis(2-pyridyl)benzene. Crystal structures of [Hg(N-C-N)Cl], [Pd(N-C-N)Cl], and $[Pd_2(N\text{-}C\text{-}N)_2(\mu\text{-}OAc)]_2$ $[Hg_2Cl_6]$. Catalytic activity in the Heck reaction. Organometallics. **24**, 53–61 (2005)
54. Donald, W.A., McKenzie, C.J., O'Hair, R.A.J.: C-H bond activation of methanol and ethanol by a high-spin $Fe^{IV}O$ biomimetic complex. Angew. Chem. Int. Ed. **50**, 8379–8383 (2011)
55. Lam, A.K.Y., Li, C., Khairallah, G., Kirk, B.B., Blanksby, S.J., Trevitt, A.J., Wille, U., O'Hair, R.A.J., da Silva, G.: Gas-phase reactions of aryl radicals with 2-butyne: experimental and theoretical investigation employing the N-methyl-pyridinium-4-yl radical cation. Phys. Chem. Chem. Phys. **14**, 2417–2426 (2012)
56. Donald, W.A., Khairallah, G.N., O'Hair, R.A.J.: The effective temperature of ions stored in a linear quadrupole ion trap mass spectrometer. J. Am. Soc. Mass Spectrom. **24**, 811–815 (2013)
57. Gaussian 09, Revision D.01, M. J. Frisch, G. W. Trucks, H. B. Schlegel, G. E. Scuseria, M. A. Robb, J. R. Cheeseman, G. Scalmani, V. Barone, G. A. Petersson, H. Nakatsuji, X. Li, M. Caricato, A. Marenich, J. Bloino, B. G. Janesko, R. Gomperts, B. Mennucci, H. P. Hratchian, J. V. Ortiz, A. F. Izmaylov, J. L. Sonnenberg, D. Williams-Young, F. Ding, F. Lipparini, F. Egidi, J. Goings, B. Peng, A. Petrone, T. Henderson, D. Ranasinghe, V. G. Zakrzewski, J. Gao, N. Rega, G. Zheng, W. Liang, M. Hada, M. Ehara, K. Toyota, R. Fukuda, J. Hasegawa, M. Ishida, T. Nakajima, Y. Honda, O. Kitao, H. Nakai, T. Vreven, K. Throssell, J. A. Montgomery, Jr., J. E.

Peralta, F. Ogliaro, M. Bearpark, J. J. Heyd, E. Brothers, K. N. Kudin, V. N. Staroverov, T. Keith, R. Kobayashi, J. Normand, K. Raghavachari, A. Rendell, J. C. Burant, S. S. Iyengar, J. Tomasi, M. Cossi, J. M. Millam, M. Klene, C. Adamo, R. Cammi, J. W. Ochterski, R. L. Martin, K. Morokuma, O. Farkas, J. B. Foresman, and D. J. Fox: Gaussian, Inc., Wallingford CT, 2016

58. Zhao, Y., Truhlar, D.G.: The M06 suite of density functionals for main group thermochemistry, thermochemical kinetics, noncovalent interactions, excited states, and transition elements: two new functionals and systematic testing of four M06-class functionals and 12 other functionals. Theor. Chem. Accounts. **120**, 215–241 (2008)
59. Andrae, D., Huermann, U., Dolg, M., Stoll, H., Preu, H.: Energy-adjusted ab initio pseudopotentials for the second and third row transition elements. Theor. Chim. Acta. **77**, 123–141 (1990)
60. Dolg, M., Wedig, U., Stoll, H., Preuss, H.: Energy-adjusted ab initio pseudopotentials for the first row transition elements. J. Chem. Phys. **86**, 866–872 (1987)
61. Petersson, G.A., Al-Laham, M.A.: A complete basis set model chemistry. II. Open-shell systems and the total energies of the first-row atoms. J. Chem. Phys. **94**, 6081–6090 (1991)
62. Gaussian 16, Revision B.01, M. J. Frisch, G. W. Trucks, H. B. Schlegel, G. E. Scuseria, M. A. Robb, J. R. Cheeseman, G. Scalmani, V. Barone, G. A. Petersson, H. Nakatsuji, X. Li, M. Caricato, A. V. Marenich, J. Bloino, B. G. Janesko, R. Gomperts, B. Mennucci, H. P. Hratchian, J. V. Ortiz, A. F. Izmaylov, J. L. Sonnenberg, D. Williams-Young, F. Ding, F. Lipparini, F. Egidi, J. Goings, B. Peng, A. Petrone, T. Henderson, D. Ranasinghe, V. G. Zakrzewski, J. Gao, N. Rega, G. Zheng, W. Liang, M. Hada, M. Ehara, K. Toyota, R. Fukuda, J. Hasegawa, M. Ishida, T. Nakajima, Y. Honda, O. Kitao, H. Nakai, T. Vreven, K. Throssell, J. A. Montgomery, Jr., J. E. Peralta, F. Ogliaro, M. J. Bearpark, J. J. Heyd, E. N. Brothers, K. N. Kudin, V. N. Staroverov, T. A. Keith, R. Kobayashi, J. Normand, K. Raghavachari, A. P. Rendell, J. C. Burant, S. S. Iyengar, J. Tomasi, M. Cossi, J. M. Millam, M. Klene, C. Adamo, R. Cammi, J. W. Ochterski, R. L. Martin, K. Morokuma, O. Farkas, J. B. Foresman, and D. J. Fox: Gaussian, Inc., Wallingford CT, 2016
63. Becke, A.D.: Density-functional thermochemistry. III. The role of exact exchange. J. Chem. Phys. **98**, 5648–5652 (1993)
64. Grimme, S., Antony, J., Ehrlich, S., Krieg, H.: A consistent and accurate ab initio parametrization of density functional dispersion correction (DFT-D) for the 94 elements H-Pu. J. Chem. Phys. **132**, 154104 (2010)
65. Grimme, S., Ehrlich, S., Goerigk, L.: Effect of the damping function in dispersion corrected density functional theory. J. Comput. Chem. **32**, 1456–1465 (2011)
66. McLean, A.D., Chandler, G.S.: Contracted Gaussian basis sets for molecular calculations. I. Second row atoms, Z =11–18. J. Chem. Phys. **72**, 5639–5648 (1980)
67. Neese, F.: Software update: the ORCA program system, version 4.0. WIREs Comput. Mol. Sci. **8**, e1327 (2018)
68. Chai, J.-D., Head-Gordon, M.: Long-range corrected hybrid density functionals with damped atom-atom dispersion corrections. Phys. Chem. Chem. Phys. **10**, 6615–6620 (2008)
69. Goerigk, L., Grimme, S.: Efficient and accurate double-hybrid-meta-GGA density functionals-evaluation with the extended GMTKN30 database for general main group thermochemistry, kinetics, and noncovalent interactions. J. Chem. Theory Comput. **7**, 291–309 (2011)
70. Kozuch, S., Martin, J.M.L.: DSD-PBEP86: in search of the best double-hybrid DFT with spin-component scaled MP2 and dispersion corrections. Phys. Chem. Chem. Phys. **13**, 20104–20107 (2011)
71. Weigend, F., Häser, M., Patzelt, H., Ahlrichs, R.: RI-MP2: optimized auxiliary basis sets and demonstration of efficiency. Chem. Phys. Lett. **294**, 143–152 (1998)
72. Weigend, F., Ahlrichs, R.: Balanced basis sets of split valence, triple zeta valence and quadruple zeta valence quality for H to Rn: design and assessment of accuracy. Phys. Chem. Chem. Phys. **7**, 3297–3305 (2005)
73. Mehta, N., Casanova-Páez, M., Goerigk, L.: Semi-empirical or non-empirical double-hybrid density functionals: which are more robust? Phys. Chem. Chem. Phys. **20**, 23175–23194 (2018)
74. McLuckey, S.A., Goeringer, D.E.: Slow heating methods in tandem mass spectrometry. J. Mass Spectrom. **32**, 461–474 (1997)
75. Dau, P.D., Armentrout, P.B., Michelini, M.C., Gibson, J.K.: Activation of carbon dioxide by a terminal uranium-nitrogen bond in the gas-phase: a demonstration of the principle of microscopic reversibility. Phys. Chem. Chem. Phys. **18**, 7334–7340 (2016)
76. Butschke, B., Schwarz, H.: Mechanistic study on the gas-phase generation of "rollover"-cyclometalated $[M(bipy{-}H)]^+$ (M = Ni, Pd, Pt). Organometallics. **29**, 6002–6011 (2010)
77. Perera, M., Metz, R.B., Kostko, O., Ahmed, M.: Vacuum ultraviolet photoionization studies of $PtCH_2$ and H-Pt-CH_3: a potential energy surface for the Pt^+CH_4 reaction. Angew. Chem. Int. Ed. **52**, 922–925 (2013)
78. Goerigk, L., Hansen, A., Bauer, C., Ehrlich, S., Najibi, A., Grimme, S.: A look at the density functional theory zoo with the advanced GMTKN55 database for general main group thermochemistry, kinetics and noncovalent interactions. Phys. Chem. Chem. Phys. **19**, 32184–32215 (2017)
79. de Bruin, B., Gualco, P., Paul, N.D.: Redox non-innocent ligands. In: Stradiotto, M., Lundgren, R.J. (eds.) Ligand Design in Metal Chemistry, vol. 33, pp. 176–204. John Wiley & Sons, Ltd, Chichester (2016)
80. Ferreira, R.B., Murray, L.J.: Group 10 and 11 transition metal-dinitrogen complexes. In: Nishibayashi, Y. (ed.) Transition metal-dinitrogen complexes: preparation and reactivity, Chapter 8, pp. 403–423. Wiley-VCH, Weinheim (2019)
81. Bond, G.C.: Relativistic phenomena in the chemistry of the platinum group metals. Effects on coordination and chemisorption in homogeneous and heterogenous catalysis. Platinum Metal Rev. **44**, 146–155 (2000)
82. Landis, C.R., Morales, C.M., Stahl, S.S.: Insights into the spin-forbidden reaction between $L_2Pd(0)$ and molecular oxygen. J. Am. Chem. Soc. **126**, 16302–16303 (2004)
83. Stahl, S.S., Thorman, J.L., Nelson, R.C., Kozee, M.A.: Oxygenation of nitrogen-coordinated palladium(0): synthetic, structural, and mechanistic studies and implications for aerobic oxidation catalysis. J. Am. Chem. Soc. **123**, 7188–7189 (2001)
84. Gómez-Gallego, M., Sierra, M.A.: Kinetic isotope effects in the study of organometallic reaction mechanisms. Chem. Rev. **111**, 4857–4963 (2011)
85. Yu, D., Tian, Z.-Y., Wang, Z., Liu, Y.-X., Zhou, L.: Experimental and theoretical study on acetone pyrolysis in a jet-stirred reactor. Fuel. **234**, 1380–1387 (2018)
86. Trentelman, K.A., Kable, S.H., Moss, D.B., Houston, P.L.: Photodissociation dynamics of acetone at 193 nm: photofragment internal and translational energy distributions. J. Chem. Phys. **91**, 7498–7513 (1989)
87. Lesslie, M., Yang, Y., Canty, A.J., Piacentino, E., Berthias, F., Maitre, P., Ryzhov, V., O'Hair, R.A.J.: Ligand-induced decarbonylation in diphosphine-ligated palladium acetates $[CH_3CO_2Pd((PR_2)_2CH_2)]^+$ (R = Me and Ph). Chem. Commun. **54**, 346–349 (2018)
88. Ly, T., Julian, R.R.: Residue-specific radical-directed dissociation of whole proteins in the gas phase. J. Am. Chem. Soc. **130**, 351–358 (2008)
89. Knoll, H., Stich, R., Hennig, H., Stufkens, D.J.: Spectroscopic studies on the mechanism of photolysis of $Pt(N_3)_2(P(C_6H_5)_3)_2$. Inorg. Chim. Acta. **178**, 71–76 (1990)